JAAS

ROYAL SOCIETY OF CHEMISTRY

PAPER

View Article Online
View Journal | View Issue

Cite this: J. Anal. At. Spectrom., 2026, 41, 1386

Elemental analysis of air-sensitive frozen molten salt samples using an inert transfer chamber for LIBS/LA-ICP-TOF-MS analysis†

Hunter B. Andrews, *[a] Peggy T. Milota, [ab] Sam Schultz,[c] Charlie Ferguson,[c] C. Derrick Quarles, Jr., [d] Supathorn Phongikaroon [b] and Benjamin T. Manard *[e]

A novel inert sample transfer system was developed and employed to enable, for the first time, the analysis of air-sensitive salt samples in a two-volume ablation cell using simultaneous laser-induced breakdown spectroscopy (LIBS) and laser ablation (LA)-inductively coupled plasma (ICP)-time-of-flight (TOF)-mass spectrometry (MS) analysis. Molten salts are of growing interest as a medium for advanced nuclear reactors and nuclear fuel reprocessing technologies continue to be developed around their use. However, compositional analysis of molten salt samples can be challenging because of their air-sensitive nature and varying solubilities leading to inaccurate measurements when digested. LA-based analysis provides an alternate method to digestion and can provide rapid elemental information with little sample preparation. In this study, LIBS and LA-ICP-TOF-MS were used to analyze the Ce content in frozen salt samples taken from a series of electrochemical experiments. Calibrations were built for each technique, and the resulting limits of detection for Ce were estimated to be 107 and 58 μg g^{-1} for LIBS and LA-ICP-TOF-MS, respectively. Test samples from the electrochemical experiments were analyzed using these calibrations. The results matched bulk digestion-based ICP-optical emission spectroscopy values, and daily trends in Ce concentration changes were identified. Additionally, the LIBS and LA-ICP-TOF-MS analysis was demonstrated for identifying microgram per gram levels of components and detecting trace contaminants. The impurities detected by LIBS included Al, Mg, Ca, and Na. The impurities detected by LA-ICP-TOF-MS included W, Ag, Al, Fe, Ni, Mo, Nd, Sm, Th, and U.

Received 2nd December 2025
Accepted 23rd February 2026

DOI: 10.1039/d5ja00482a

rsc.li/jaas

1 Introduction

Interest in molten salts has increased with the growing interest in advanced nuclear reactor designs and reprocessing of used nuclear fuel (UNF). Molten salt reactors (MSRs) are an advanced nuclear reactor design in which fissile fuel is dissolved into the working fluid in the form of a molten salt.[1–3] Using molten salt media provides increased thermal efficiency in the reactor and passive safety features, such as passive recirculation and subsequent freezing in case power is lost. However, one of the challenges associated with molten salts relates to corrosion. When corrosion occurs, structural alloys and other components degrade, and resultant impurities (*e.g.*, Cr) are dissolved in the salt. Additionally, the nuclear reactions generate a range of fission products in the liquid salt.[4–6] These fission products and corrosion species may deposit on structural materials, form aggregates in the salt, or volatilize into the gas phase, which requires capture in the off-gas system.[7] Lastly, since fuel material is dissolved into the bulk salt, quantifying the fuel concentration in salt (*e.g.*, U) is of interest to understand the ongoing state of the reactor.

Molten salt reprocessing, or pyroprocessing, involves using molten salts in a batch process electrochemical cell (*i.e.*, electrorefiner).[8,9] UNF is typically dissolved into the high-temperature salt (*e.g.*, LiCl–KCl eutectic) and then recovered on solid or liquid cathodes while separating fission products. Similar to MSRs, corrosion of the electrorefiner vessel is a concern for pyroprocessing applications, and the composition of the salt itself can have a range of impurities (*e.g.*, transition

[a]Radioisotope Science and Technology Division, Oak Ridge National Laboratory, Oak Ridge, Tennessee, USA. E-mail: andrewshb@ornl.gov
[b]Department of Mechanical and Nuclear Engineering, Virginia Commonwealth University, Richmond, Virginia, USA
[c]Elemental Scientific Lasers, Bozeman, Montana, USA
[d]Elemental Scientific Inc., Omaha, Nebraska, USA
[e]Chemical Sciences Division, Oak Ridge National Laboratory, Oak Ridge, Tennessee, USA. E-mail: manardbt@ornl.gov

metals, lanthanides) because of the varying fission products within the UNF.[10]

For both MSRs and pyroprocessing applications, accurate and timely compositional analysis of the salt is critical, yet fraught with challenges.[11] *In situ* approaches using electrochemistry,[12] absorbance spectroscopy,[13] and laser-induced breakdown spectroscopy (LIBS)[14,15] are currently being investigated. Compact electrochemical sensors have been developed to quantify fuel material and corrosion product impurities in the salt by measuring the electrical potential or current produced when target species undergo redox reactions.[12] Absorbance spectroscopy has been explored for quantifying U concentration and oxidation states in the salt providing real-time results; however, this method traditionally requires transparent windows in contact with the salt which is problematic for fluoride salts which etch most materials.[13] Online LIBS measurements have been demonstrated through aerosolizing molten salts; this approach allows for continuous real-time monitoring but sampling through aerosolization may dilute trace analytes below detection limits.[14,15] Generally, these methods are aimed toward online monitoring and either have larger associated uncertainties or are only sensitive to specific species in the salt. Traditional analytical methods applied to the samples employ radiation-based techniques,[16] inert gas fusion,[17] and inductively coupled plasma-mass spectrometry (ICP-MS) or ICP-optical emission spectroscopy (OES).[11,18] Traditionally, ICP-based measurements rely on digestion of frozen salt samples, which can be cumbersome because of the formation of fluorides and oxides that are insoluble in HNO_3 or HCl, leading to precipitation. The halide salts used for MSRs and pyroprocessing are also air-sensitive, meaning their reactions with air can affect their solubilities. Finally, some salt species (*e.g.*, I, Te, Se) may be volatile, resulting in their loss during transport, grinding, or digestion.

To alleviate the need for digestions, an alternative approach could be direct solid sampling, such as laser ablation (LA). LA-ICP-MS is performed by ablating a solid sample with a laser pulse and directing the ablated material into an ICP-MS instrument for analysis.[19] LA-ICP-MS is commonly employed to circumvent the digestion of materials for ICP-MS analysis, particularly for heterogeneous materials such as geological samples. LA-ICP-MS has been used for analyzing coupons exposed to molten salts, providing spatial information related to alloy components within the slat residue on the surface of the coupons.[20] However, LA-ICP-MS has not been demonstrated for measuring the frozen salts themselves. Additionally, within the laser pulse from LA-ICP-MS, the optical emissions can be measured to determine elemental compositions (*i.e.*, LIBS).[21] This allows LIBS and LA-ICP-MS to be performed simultaneously, providing a wealth of analytical information.[22] LIBS and LA-ICP-MS are very complementary techniques; LIBS provides strong sensitivity to light elements (*e.g.*, H, C, O, Li), whereas LA-ICP-MS excels at the detection of heavy elements, isotopes, and generally has better sensitivity for trace elements. Furthermore, the simultaneous use of the two techniques allows for an extended dynamic detection range. For example, if the LA-ICP-MS saturates due to high concentrations of a given element, LIBS will likely be able to detect one of the many emission peaks still within its dynamic range. These complementary strengths are particularly advantageous for frozen salt samples, as they allow for the detailed resolution of zone freezing effects[23] and the precise characterization of both light and heavy elements, ultimately leading to more accurate compositional analysis.

While LA-ICP-MS has not been demonstrated for frozen salts, LIBS has been previously used in this manner. LIBS studies performed with inert sample cells/environments have been demonstrated several times in the literature but have been limited by the challenges of dust accumulation and optical alignment consistency. Williams *et al.* measured Ce in frozen LiCl–KCl salts by loading samples into glass vials in a glovebox and sealing them for removal and analysis. This approach achieved LOD for Ce of 0.099 wt% (990 $\mu g\ g^{-1}$), but the study found challenges with dust accumulation within the glass vials during LIBS analysis.[24] Two follow-on studies from Andrews and Phongikaroon designed a similar LIBS system within the sample preparation glovebox to avoid issues with removal and the glass vials.[25,26] Hull *et al.* investigated the use of LIBS to quantify Pr, Ho, and Er in LiCl–KCl salts achieving LODs as low as 300 $\mu g\ g^{-1}$, but challenges associated with moisture exposure in the sealed cell used was mentioned.[27] The final study from Myhre *et al.* investigated the penetration of FLiNaK and FLiBe salts into graphite specimens.[28] These were loaded into an inert sample cell in a glovebox and then transferred to a LIBS instrument. This cell could maintain an inert cover gas during analysis to prevent dust accumulation on the window and moisture challenges were not reported. The study from Myhre *et al.* used a sample chamber compatible with LA-ICP-MS measurements (*i.e.*, one-volume cells). However, none were of the current state-of-the-art, two-volume design, which has benefits related to washout and sensitivity.[28] In this study, a novel inert transfer chamber was explored to extend the capabilities of two-volume ablation cells to be able to measure air-sensitive samples. The inert transfer chamber permits sample preparation and analysis in separate spaces with little concern for the atmospheric conditions when moving samples between locations.

LA-ICP-MS may be able to achieve greater figures of merit compared with LIBS—particularly with heavier elements and the added benefit of isotopic analysis. For the LA-ICP-MS in this study, a time-of-flight (TOF) mass analyzer was used, which permits quasi-simultaneous measurements of all nuclides from ^{6}Li to ^{238}U. This instrument was used to allow an untargeted data screening tool to be used to investigate minor components/inclusions in the salt samples.

Thus, the primary goals of this study were to (1) demonstrate the effectiveness of an inert sample transfer system for LA-ICP-MS measurements, (2) evaluate and compare the capabilities of LIBS and LA-ICP-TOF-MS in analyzing the Ce concentration in frozen LiCl–KCl salt samples, and (3) apply the resulting calibration protocols to a set of samples obtained from a molten salt electrochemical experiment. Here, LIBS and LA-ICP-MS were performed simultaneously. This allowed permitted both moisture/light element detection (LIBS) and compositional/

isotopic screening (LA-ICP-TOF-MS) in a single analytical run, minimizing sample exposure and maximizing the depth of data collected in a short time. Furthermore, by performing both simultaneously, a fairer comparison between the Ce quantification of both methods can be made by sampling the exact same portion of the sample. The outcome is a robust, high-throughput analytical workflow tailored to accurately capture the diverse chemical signatures relevant to the molten salt community.

2 Experimental

2.1 Samples

All sample preparation was performed in a glovebox with a maintained Ar atmosphere (<5 ppm for H_2O and <1 ppm O_2). A mixture of LiCl (ultradry, 99.9%, Thermo Fisher Scientific, Germany) and KCl (ultradry, 99.9%, Thermo Fisher Scientific) was prepared at the eutectic point (59 : 41 mol% LiCl : KCl) as the base salt for all samples. Various mixtures of $CeCl_3$ (ultradry, 99.9%, Thermo Fisher Scientific) in the LiCl–KCl eutectic were prepared to form the calibration dataset. The salts were loaded into crucibles and dried at 250 °C for >2 h, then raised to 500 °C and left to melt and further dehydrate overnight.[29] This step is important for the removal of any free moisture from the salt. Salt was sampled in the form of frozen ingots (nominally 4 mm in diameter). This sampling was performed using a syringe attached to a glass tube (4 mm inner diameter).[24,26] Approximately 0.5 mL of salt was rapidly withdrawn into the glass tube, and the salt subsequently froze. Note that the salt ingot formation was performed manually and variation in the glass tube diameter and withdrawal rate introduce some uncertainty. Future work could automate this with high precision glassware to minimize this uncertainty. The frozen ingots were removed from the glass rods, inspected to ensure a solid ingot was formed without major surface defects, and sealed in individual containers until analysis (Fig. S1).

For electrochemical tests, a 35 g blend of nominally 5700 μg Ce (as $CeCl_3$) per g of LiCl–KCl was prepared using the same procedure. The corrosion rates of different Al coupons, with and without passivation layers (control and treated, respectively), were measured using open circuit potential, electrochemical impedance spectroscopy, and linear sweep voltammetry over the course of several days.[29] Additional details are provided in the SI. For these electrochemical tests, the working electrode was a control or treated Al 6061 coupon held in a Mo wire basket, the counter electrode was a W rod, and a 1 mol% Ag/AgCl reference electrode was used. During the electrochemical measurements, sample salt ingots were collected before the experiment and then on each subsequent day to investigate the depletion of Ce from the salt as an effect of the corrosion mechanisms. A list of salt samples and their ICP-OES measured concentrations are provided in Table 1.

Table 1 ICP-OES bulk-digestion compositions of the calibration samples[a]

	Prepared
Sample	Ce[b] (μg g^{-1})
Blank	<DL[c]
1	962 ± 91
2	2373 ± 222
3	3593 ± 340
4	5134 ± 480

[a] Balance of salt composition is LiCl–KCl eutectic. [b] As measured by ICP-OES. [c] DL = detection limit.

2.2 Equipment

LIBS and LA-ICP-MS were performed using an ImageGEO193 LA system (Elemental Scientific Lasers [ESL], USA). The 193 nm excimer laser is fired into a He-purged (ultrahigh purity, 99.999%, Airgas, USA), 800 mL min^{-1}, two-volume (TwoVol3, ESL) LA cell. Salt samples were loaded into a novel inert chamber (AirLOCK, ESL) for transporting from the glovebox and loading into the two-volume ablation cell. Additional details on the AirLOCK usage are detailed below.

The LIBS cup contained two embedded optical fibers to transmit the plasma light from the laser-induced plasma to the spectrometers for LIBS measurements.[22] The first spectrometer was a five-channel (188–1099 nm), complementary metal–oxide semiconductor (CMOS)-equipped spectrometer. The second spectrometer was a 0.32 m Czerny–Turner spectrometer equipped with an intensified charge-coupled device (ICCD) detector. For both spectrometers, the delay and integration were set to 0.1 μs and 1 ms, respectively. This was selected based on a brief tuning of the LIBS spectrometers using the most concentrated calibration sample. This was accomplished by tuning the LIBS parameters to maximize the Ce signal while minimizing the continuum background (*i.e.*, maximize signal-to-noise ratio). The most concentrated calibration sample was used to ensure the ICCD spectrometer did not saturate within the calibration range. The ICCD spectrometer was centered at 572 nm using a 1800 lines per millimeter grating blazed at 500 nm.

The ablation cell was optimized for LA-ICP-TOF-MS sensitivity and washout resulting in the He carrier gas being operated at 800 mL min^{-1}. The ablated material was transported from the ablation cup through polyvinyl chloride tubing (Tygon Formulation B44-4X, France) to an ICP-TOF-MS (icpTOF R, TOFWERK AG, Switzerland). For efficient introduction into the ICP, a dual concentric injector (DCI2, ESL) was used with a 796 mL min^{-1} sample gas (Ar).

All measurements were made with approximately 1.4 mJ at each pulse (14 J cm^{-2}). All measurements were performed as line-scans with a spot size of 100 × 100 μm and 10 μm lateral movement between spots (90% overlap). This was accomplished by maintaining a 50 Hz repetition rate and moving the stage as a speed of 500 μm s^{-1}. Analytical measurements were made on a line-scan after it had been previously ablated as to sample the interior of the salt ingot.

2.3 Bulk digestion ICP-OES/MS analysis

To benchmark Ce concentrations in the calibration dataset and comparative values for the test samples, samples were analyzed using ICP-OES. Approximately 10 mg of the salt ingots were

gravimetrically digested in 1 mL of 5% HNO_3 in Savillex vials. The vials were heated to 100 °C for 1 hour on a hot plate, then gravimetrically diluted 100×, and analyzed using ICP-OES (iCAP PRO, Thermo Scientific, Germany). The results were then corrected for dilutions and the mass of salt digested. The same digested samples were analyzed using a triple quadrupole (TQ) ICP-MS (iCAP TQ, Thermo Scientific) for verification of trace impurities.

2.4 Data analysis

ICP-TOF-MS data reduction and LIBS peak integration were performed using iolite 4 software (ESL).[30] Weighted linear regression calibrations were built using the NumPy and SciPy libraries in Python 3. ICP-TOF-MS data screening was performed using the open source TOFHunter program (https://github.com/andrewshb/TOFHunter).[31] TOFHunter applies principal component analysis (PCA) to identify major variance sources and their correlations. Additionally, TOFHunter applies the interesting features finder (IFF) algorithm to ICP-TOF-MS to locate unique mass spectra that may not contribute a major source of variance to the dataset but still represent a distinctive signature among the data.

3 Results and discussion

3.1 Performance of AirLOCK chamber

One-volume LA cells have been capable of being loaded in inert environments for some time because of the cell mounting on top of the motorized stages used for LA.[28] However, the integrated stages in two-volume ablation cells prohibit transporting the ablation cell itself because of its size.[32] This study examined using the AirLOCK inert transfer system for loading air-sensitive samples into a two-volume ablation cell. Salt ingots were first loaded onto a measurement tray (Fig. S2) in an Ar atmosphere glovebox. The measurement tray (max sample size: 76 mm × 100 mm × 10 mm) was then sealed into the AirLOCK transfer system before removal from the glovebox. The sealed AirLOCK system was transported approximately 1.6 km (encompassing 30 min in approximately 69% relative humidity) to the analytical laboratory and then integrated into the ImageGEO193 (ESL). The AirLOCK was attached (while still sealed) to the loading door of the TwoVol3 chamber (Fig. S3). Next, the two-volume ablation cell was purged with He for instrument default time (120 s). The TwoVol3 ablation cell pressure was properly maintained during the purge process, indicating that the AirLOCK system properly sealed to the front of the ablation system. Subsequently, the door between the AirLOCK and two-volume ablation cell was remotely opened so the sample tray could be loaded fully into the ablation chamber without air exposure. The salt sample preparation, loading process, and test ablation cell diagram is visualized in Fig. 1.

To evaluate the performance of the TwoVol3 with the AirLOCK mounted, typical LA-ICP-TOF-MS tuning was completed. This consisted of rastering (10 × 10 μm) line-scans at 10 μm s^{-1} on National Institute of Standards and Technology 610 glass

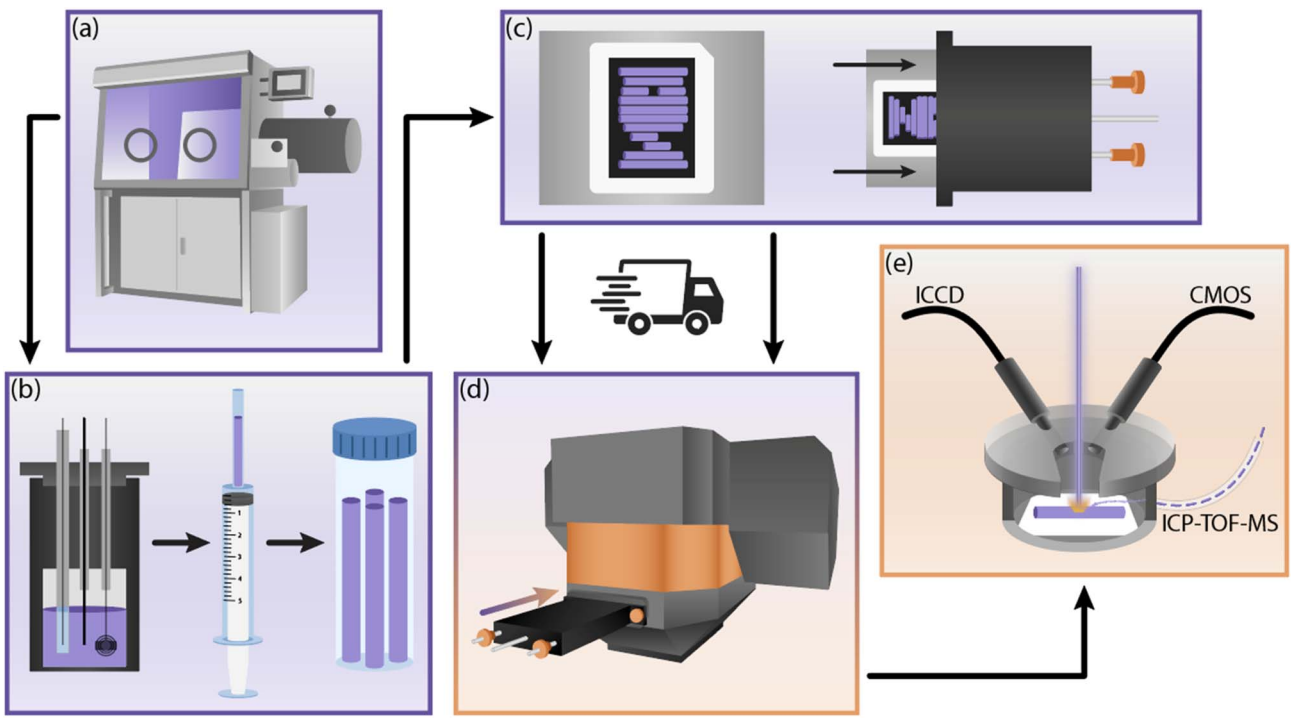

Fig. 1 Overview of experimental procedure. Salt preparation, electrochemical tests, and sampling was completed in (a) an Ar atmosphere glovebox. The salt sampling process using syringe drawn liquid salt and subsequent freezing is shown in (b). Next, the ablation tray was loaded with sample and sealed into the AirLOCK cell in the glovebox (c). The samples were then transported 1.6 km to an analytical laboratory. The AirLOCK device was connected to the laser ablation unit (d) and then purged with He before the samples were fully inserted into the unit. Lastly, (e) the samples were tested using simultaneous LIBS/LA-ICP-TOF-MS. Note: Purple boxes indicate the process happening within an Ar atmosphere glovebox and orange boxes represent the transition to the analytical laboratory and the change to a He atmosphere.

and tuning the respective gas flows (chamber and sample). Once optimized, the washout was determined to be 20 ms *via* monitoring the single pulse response (from 10 × 10 μm) ablation events. The tuning for instrument sensitivity and washout was similar to the normal operation conditions with Tygon tubing from the LA cell to the ICP-TOF-MS.

Before developing calibrations, preliminary LIBS spectra of the salt samples were examined. Because of the hygroscopic nature of chloride salts, the exterior surface of the solids absorbs moisture, even in environments with trace H_2O and O_2.[6] Previous solid salt LIBS studies used replicate shots of discrete locations,[24–27] in this study, line-scan analysis was investigated. The laser focal point was positioned on the apex of the curvature of each salt ingot and ablated with a line-scan (spot size: 100 × 100 μm, 90% overlap, 50 Hz, 500 μm s^{-1}). This was performed to better capture any variance in the composition of the frozen salt samples and any particulates or zoning features. Fig. 2 shows example normalized LIBS spectra from the first 20 shots of a line-scan of the outer surface of a 5134 ± 480 μg Ce per g salt sample measured on the CMOS spectrometer.

All major emission peaks (Ce, Li, K, and Cl) were identified. Because the bulk of the salt was eutectic LiCl–KCl, the major Li and K emissions show self-reversal behavior,[33] preventing use for analytical measurements. Despite the self-reversal effects, many weaker emission peaks provide useful peaks for Li and K (*e.g.*, K at 405 nm and Li at 810 nm). As is typical for lanthanide emission peaks, Ce lines appear as clusters of small emission lines in the 400–600 nm range.

The presence of H and O on the surface was verified when examining the first shot of each line scan (Fig. 2). Measuring H and O concentrations in salts is a difficult analytical challenge typically requiring inert gas fusion measurements.[17] Although not the focus of this study, the spectra in Fig. 2 demonstrate the feasibility of using LIBS for measuring moisture impurities in salts. This measurement capability is critical for molten-salt systems where even trace H and O can shift redox chemistry, generate oxyhalide/hydrolysis products, and accelerate alloy corrosion. Furthermore, this capability complements LA-ICP-MS, which cannot reliably detect H and has limited sensitivity to O. In addition to the surface moisture impurities, the exterior surface of the salt ingot appears to have an elevated Ce concentration, likely caused by zone freezing effects. Notably, using a small step between successive shots (10 μm) after the first shot, nearly all ablated material did not come from the salt surface, and none of the surface artifacts were observed in subsequent spectra. This result supports the need for an ablation-based technique where the surface can be removed and such that the interior of the salt ingot is sampled. To eliminate the impact of any surface moisture effects on the data collected, all line scans were completed twice with the second pass being used as the analytical measurement.

Following the calibration and testing measurements discussed in the following section, the samples were removed from the AirLOCK system and allowed to sit in open air for approximately 30 min. Within a few minutes, visible hydration was observed as a visibly wet film on the surface of the salt

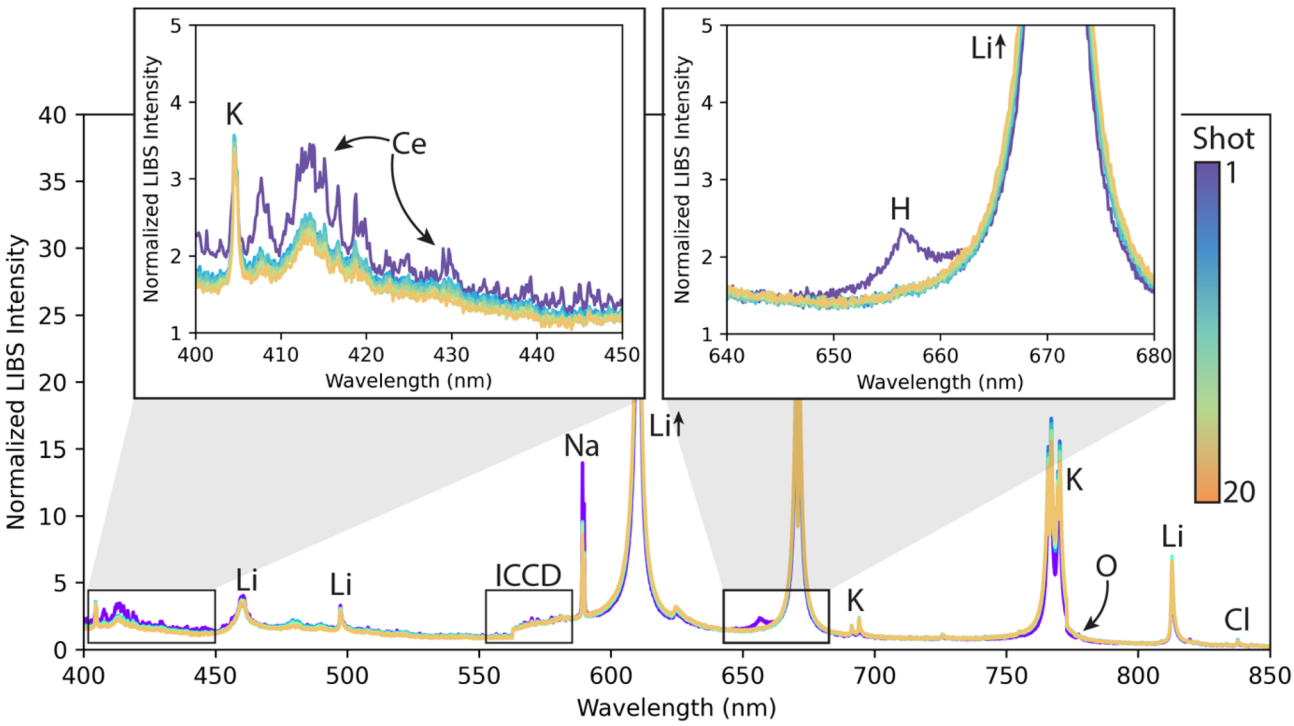

Fig. 2 Normalized LIBS spectra from the first 20 shots measured on 5133 μg Ce per g of LiCl–KCl eutectic salt using the broadband CMOS spectrometer. Surface H and concentrated Ce is shown in the first spectrum; demonstrating surface contamination by H_2O and non-uniform Ce distribution due to zone freezing. Successive shots with 90% overlap sample the homogeneous interior reducing surface effects. All analytical data was measured on a second line scan so as to only sample the interior of the salt samples. The region where the ICCD was targeted is highlighted near 570 nm.

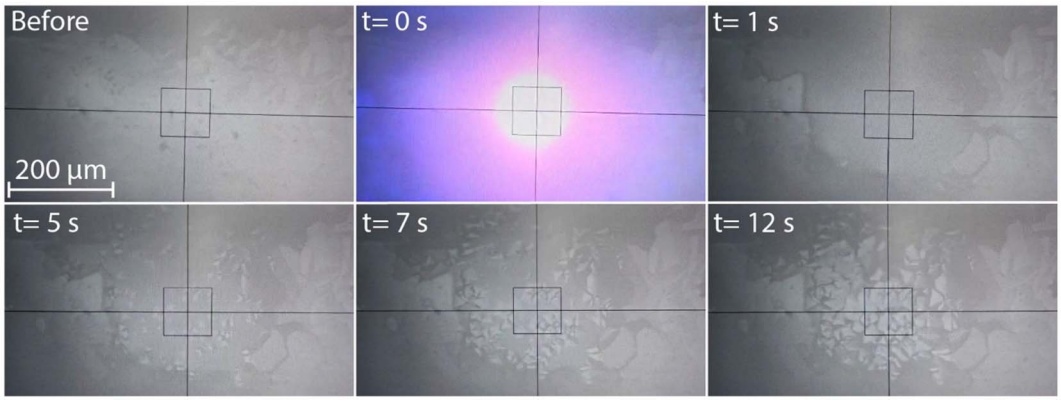

Fig. 3 Time-lapse of ablation of salt samples after exposure to air. The ablation resulted in large material loss, splashing, and subsequent recrystallization. Air exposure forms a surface brine layer, leading to destructive splashing and recrystallization during ablation, preventing reliable analysis.

ingots. The samples were reloaded into the two-volume ablation cell to test samples exposed to air, but because of splashing effects, the analysis could not be performed. A time-lapse of the ablation behavior of the salt samples after air exposure is shown in Fig. 3. The air exposure likely resulted in a thin film of brine on the surface. When ablation occurred, heat caused the salt content in the film to become enriched; then, upon cooling, the salt that was supersaturated in the brine began to crystallize on the sample surface. The optical window from the LIBS cup was investigated, and visible splashing residue was apparent. This result indicates the importance of the AirLOCK for transferring and loading air-sensitive samples into the ablation unit. However, it is important to note that the AirLOCK should not be considered for long duration sample storage. This study has demonstrated its efficacy for sample transport between an inert glovebox and an analytical laboratory, but extended use may result in the seal being compromised.

3.2 Ce quantification

A set of five calibration samples containing varying concentrations of $CeCl_3$ in LiCl–KCl was prepared to provide matrix matched standards. The salt ingots were measured using line-scans of varying lengths based on the available sample size. All measurements were made with approximately 1.4 mJ at each pulse (14 J cm^{-2}), with the number of shots per sample ranging from 700 to 2350 depending on the length of the line-scan. Although the broadband CMOS spectrometer was able to detect Ce peaks in the most concentrated sample, the emissions were weak and had a low signal-to-noise ratio. Ce emissions in less concentrated samples were not effectively resolved by the CMOS spectrometer. The ICCD spectrometer provided far greater sensitivity and was focused onto the 564–580 nm window, which contains many strong Ce emission peaks (Fig. 4). Although the CMOS spectrometer lacked the sensitivity needed at lower concentrations, it may be a viable approach for more concentrated samples and still provides broad elemental information (*e.g.*, Li, K, H, O, *etc.*). Note that more complex salt mixtures would likely give rise to interfering LIBS emission peaks. Future work should explore methods to overcome this challenge through identification of interference free peaks, peak deconvolution, or multivariate calibrations.

LIBS and LA-ICP-TOF-MS calibrations were performed simultaneously. The samples were scanned at 50 Hz. The frozen salt samples showed no indication of degradation from

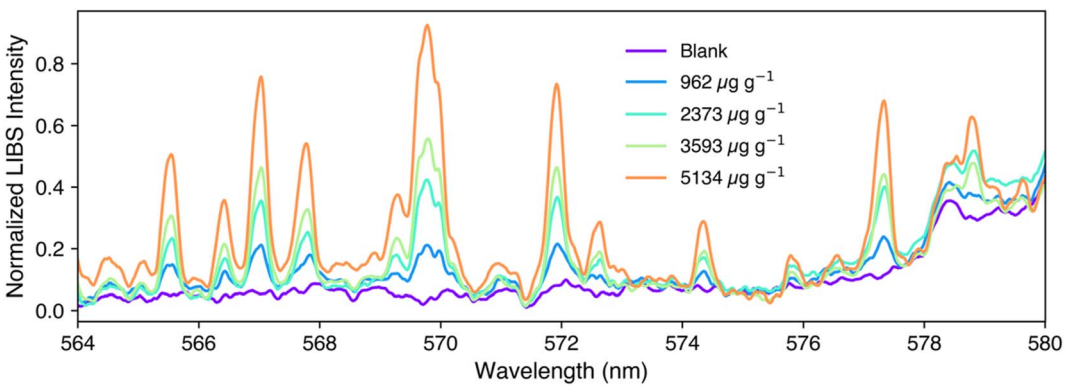

Fig. 4 Averaged and normalized LIBS spectra of the calibration set measured on the ICCD spectrometer. The emission peaks between 569–570 nm correspond to three Ce peaks not fully resolved by the spectrometer used due to their close emission wavelengths. The shoulder of salt matrix emission peak can be seen beginning at 578 nm.

repeated testing. For LIBS calibrations, selected emission peaks (567, 570 cluster, and 572 nm) were integrated and background subtracted by using the average of three data points to the left and right of the integrated area. LA-ICP-TOF-MS calibrations were baseline corrected using the gas blanks between line-scans.

A weighted linear regression was used because for both instruments the variance increased with signal intensity. This heteroscedastic nature relates to the signal originating by counting discrete photons or ions whose generation is itself stochastic and concentration-dependent. Weights were set inversely proportional to the sample-measurement variance, appropriate when variance increases with signal (heteroscedasticity). This method was recommended in several literature studies for use when the variance scales with concentration as it does in this study.[34,35] The limits of detection (LODs) and limits of quantification (LOQs) were determined using the 95% prediction intervals of the linear model, as described by Mermet.[34] This approach considers the calibration uncertainty and incorporates signal dependent variance to provide a realistic LOD. The optimal LIBS and LA-ICP-TOF-MS calibrations, along with figures of merit, are shown in Fig. 5.

Generally, this calibration procedure demonstrates that multiple LIBS and LA-ICP-TOF-MS signatures can be used to adequately quantify Ce in salt samples. Phongikaroon and Simpson reported the anticipated lanthanide concentrations in pyroprocessing salts after treatment to range from approximately 100–10 000 μg g^{-1}.[36] Thus, the LODs demonstrated in this study are at a level at which they would be applicable to Ce and potentially a range of similar analytes in pyroprocessing molten salt samples. Additionally, the LIBS LOD represents an 89% reduction in the Ce LOD compared with the previous study from Williams *et al.* in chloride salts.[24] It also represents a significant improvement in LODs for impurities compared to other studies investigating detection of various lanthanides[25–27] in frozen salt samples. The LA-ICP-TOF-MS method provides a 50% improvement in detection capabilities compared to the LIBS method. While these LODs were determined using the prediction interval approach, the detection limits calculated using the typical 3-sigma method ($LOD_{3\sigma}$) were 103 and 19 μg g^{-1} for the 570 nm LIBS and ^{142}Ce LA-ICP-TOF-MS signals, respectively. These values were calculated for future literature comparisons but also highlight the difference in sensitivity (slope intensity) between the LIBS and LA-ICP-TOF-MS measurements.

Two sets of test samples from electrochemical experiments were quantified using the top LIBS/LA-ICP-MS calibrations. The model-predicted concentrations are shown in Fig. 6, along with the ICP-OES validation measurements. The day 2 sample from the treated sample was damaged during the ingot formation, so it was excluded. *Z*-scores were calculated for each sample to compare the predictions from bulk digestion ICP-OES, LIBS, and LA-ICP-TOF-MS. Nearly all samples agree well between the three methods, having *Z*-scores with an absolute value less than two. However, the LIBS and LA-ICP-TOF-MS results tend to predict slightly lower Ce concentrations compared to ICP-OES measurements. This may be related to concentrated Ce inclusions or Ce precipitates, which were captured by bulk digestion but not the surface sampling technique such as LA sampling. This may be an advantage of LA sampling because molten salt characteristics (*e.g.*, diffusion coefficients, redox potential) depend on dissolved species, not insoluble elements that precipitate out of solution.

The control experiment shows no appreciable day-to-day concentration change, whereas the treated experiment shows an appreciable decrease in Ce concentration over the duration of the experiment. This decrease can be attributed to the treated cathode material resulting in increased Ce retention after reduction of the $CeCl_3$ as metal onto the cathode. These details will be further explored in a separate study; the results in the present study exemplify the capability of both LIBS and LA-ICP-TOF-MS to quantify salt composition without digestion.

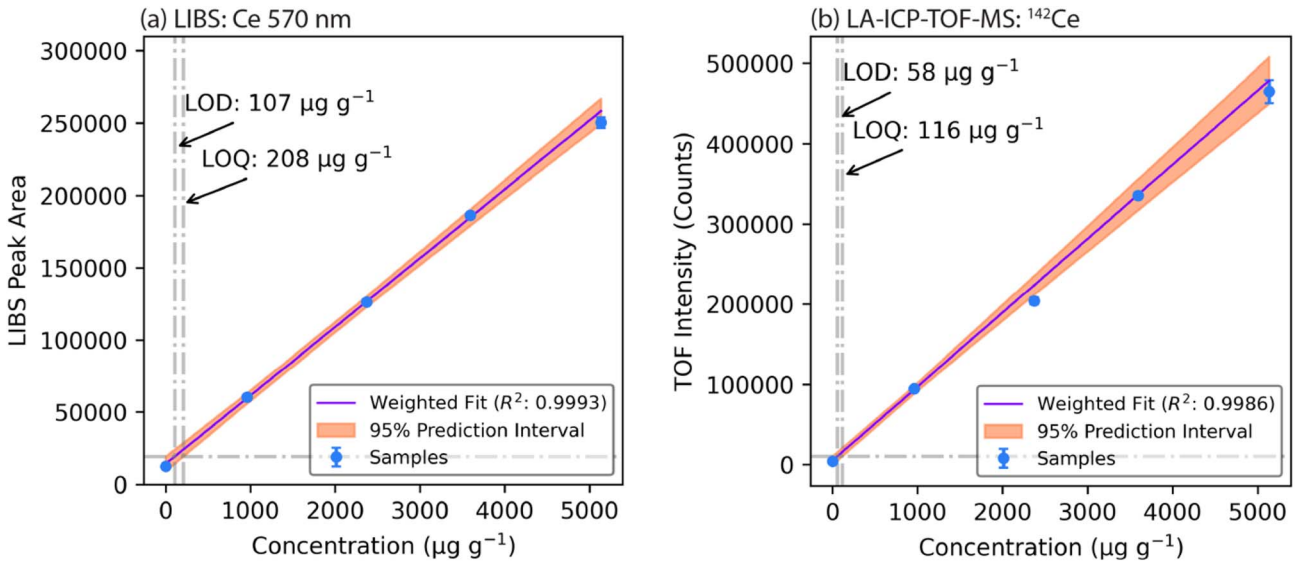

Fig. 5 Top (a) LIBS and (b) LA-ICP-TOF-MS calibrations for Ce in LiCl–KCl salts. The error bars represent 2× standard error of the mean signal.

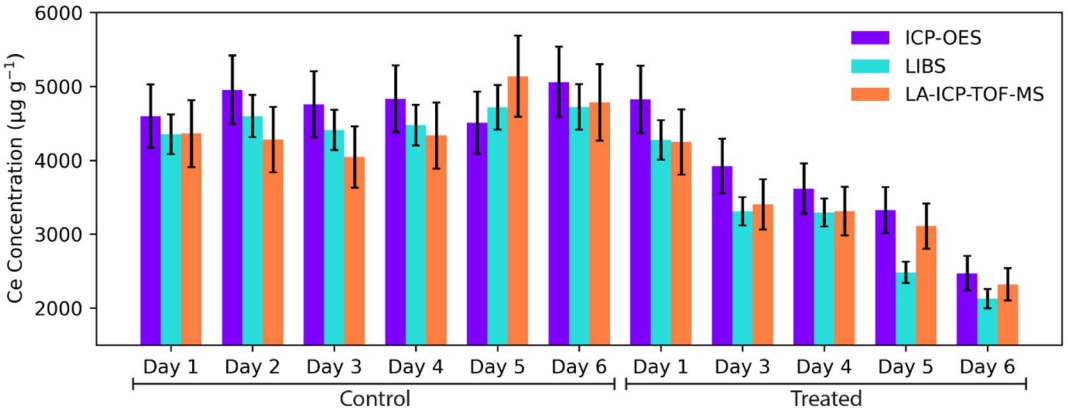

Fig. 6 Comparison of analytical measurements for Ce concentration in daily salt samples from two corrosion experiments.

3.3 Untargeted screening of LA-ICP-TOF-MS data

Beyond quantifying elements in the salt sample, qualitative elemental presence in salt samples would be of interest to the molten salt community. While the LA-ICP-MS measurements in this study could also be performed with a traditional ICP-TQ-MS, the ICP-TOF-MS provides quasi-simultaneous detection of nearly all nuclides within a single shot. In this study, the ICP-TOF-MS was employed for untargeted data screening of the salt samples using the TOFHunter program.[31] The TOFHunter program was developed at Oak Ridge National Laboratory to screen ICP-TOF-MS data to rapidly investigate major sources of variance using PCA and minor/unique sources of variance using IFF. Typically, PCA will identify the major phases of the sample, while IFF will identify distinctive inclusions or particles that are sparsely distributed through the data set. Selected mass regions of the TOFHunter PCA analysis are shown in Fig. S4–S6 in the SI. Here, PCA identified two components explaining 99.9% of the dataset variance. The first principal component (PC) largely corresponds to Ce and shows positive correlations with other elements, including Ba, Nd, and Sm (Fig. S4 and S5). The second PC is mainly positively associated with W and Ag, with very small loadings on Al, Fe, Ni, Mo, Th, and U (Fig. S4 and S6). Additionally, this second PC is slightly anticorrelated with Ce. IFF identified unique mass spectra that generally show the same information.

This screening analysis offers several insights into the samples that may have otherwise been missed when focusing on Ce. First, the $CeCl_3$ salt that was used likely had trace impurities of other lanthanides. These additional lanthanides may have overlapping masses with Ce but can be identified by considering the mass peaks observed and natural isotope ratios of nuclides sharing these masses. The second PC draws attention to some minor impurities that exist in the samples, all with logical explanations. The Al, Fe, Ni, Mo, Ag, and W would have originated from the electrode materials. While cycling the

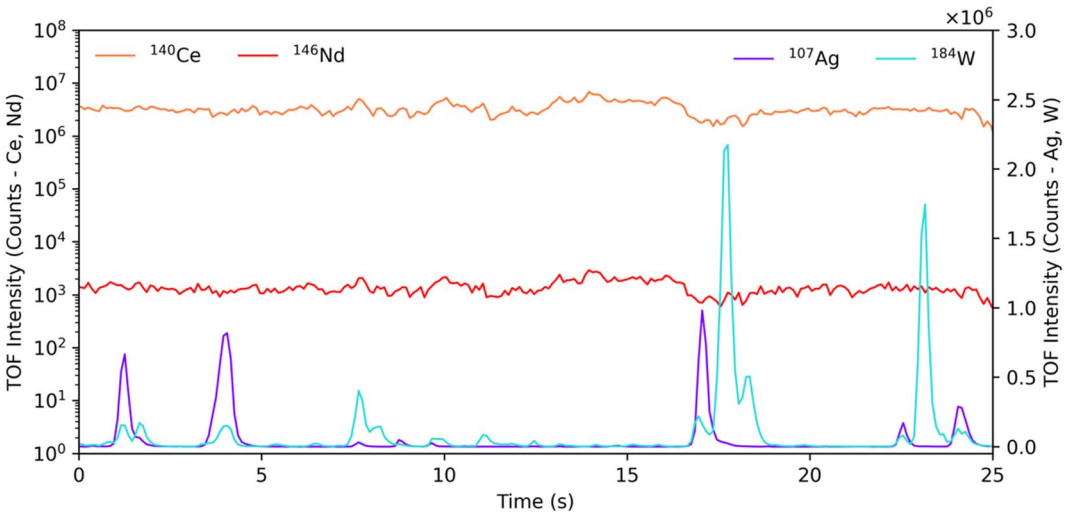

Fig. 7 Time trace of LA-ICP-TOF-MS signal over the line-scan of control sample day 6. The ^{146}Nd signal follows the trend seen by the ^{140}Ce, appearing distributed throughout the salt sample. Meanwhile, electrode signatures (^{107}Ag and ^{184}W) appear as sparse events indicating they are present as particulates within the salt. This behavior matches variance described by the PCA results shown in Fig. S4, where Nd is correlated with Ce while the electrode materials are not.

potential in the molten salt cell, the electrode materials may deteriorate. In Fig. S4–S6 the PC2 loadings show that these electrode masses are anti-correlated to the Ce masses, indicating that they are not homogeneous throughout the salt and their presence in each laser shot is independent of Ce intensity. To further investigate this, the LA-ICP-TOF-MS time traces were examined. The time trace for the control sample day 6 is shown in Fig. 7. Here, it was verified that the Ba, Nd, and Sm signatures follow the Ce signal. Furthermore, Ag and W appear as isolated particulate events throughout the line-scan, behaving independently of the Ce signal. These particulate events were not seen in the calibration dataset, nor prior to the day 6 sample; this behavior agrees with electrode degradation from repeated cycling.

The salt samples were prepared in a glovebox containing U and Th salts, so the presence of these is likely a minor contaminant. Notably, some test samples had visible dark spots against the bulk white $CeCl_3$–LiCl–KCl salt (see Fig. S2). The presence of these impurities was verified through analysis on an ICP-TQ-MS, with most being at concentrations of nanograms per gram to low micrograms per gram. However, if these impurities originated from particulates in the salt, the bulk-digestion ICP-TQ-MS may not properly capture this behavior since its measured concentration would be diluted by the bulk salt. The LA-ICP-TOF-MS untargeted screening only provides qualitative insights into the impurities, but this data can be valuable from a research perspective to investigate interactions between the salts and wetted materials (*e.g.*, electrodes or vessel walls).

4 Conclusion

Analytical measurements of samples taken from molten salt systems can be challenging because of their hygroscopic nature and issues associated with varying solubilities. Using a novel inert sample transfer system, these air-sensitive salts were transported 1.6 km to an analytical lab for measurement. While LIBS has been performed on frozen salts previously, this was the first measurement of air-sensitive salt using LA-ICP-TOF-MS. Furthermore, for the first time, air-sensitive salt samples were analyzed with both LIBS and LA-ICP-TOF-MS in a two-volume ablation cell. Thus, future work can expand upon this capability by further exploring the capabilities of these methods such as elemental imaging for inert samples.

This study demonstrated both LIBS and LA-ICP-TOF-MS as an alternative method for measuring impurities in frozen salt samples. Here, the LIBS analysis was significantly better (89% improvement in LODs) compared to previously reported LIBS efforts for quantifying Ce in frozen salt samples.[24] Furthermore, the use of LA-ICP-TOF-MS provided a further 50% reduction in Ce LOD compared to LIBS. The benefits of solid sample analysis, including the identification of surface moisture and particulate impurities, were demonstrated. Using this methodology, future studies can explore the analysis of more complex salt samples relevant to MSRs and pyroprocessing with the AirLOCK transfer system. These future studies should focus on not only additional analytes of interest, but also mixed lanthanides to simulate the anticipated fission product ratios from irradiated salt. Additionally, future work may explore the capability for moisture measurements of salts using LIBS.

Author contributions

Conceptualization (H. B. A.), data curation (H. B. A., P. T. M., B. T. M., C. D. Q.), formal analysis (H. B. A., B. T. M.), funding acquisition (H. B. A., S. P., B. T. M), investigation (H. B. A., P. T. M., B. T. M., C. D. Q.), methodology (H. B. A., B. T. M., C. D. Q., S. S., C. F.), visualization (H. B. A.), writing – original draft (H. B. A.), writing – review & editing (all authors).

Conflicts of interest

S. S., C. F., and C. D. Q. were employees of Elemental Scientific Inc. at the time of this study.

Data availability

All relevant data that support these experimental findings are available from the corresponding author upon reasonable request.

Supplementary information (SI) including information on the electrochemical tests performed, salt sample preparation, images of the samples and AirLOCK system, and TOFHunter results is available. See DOI: https://doi.org/10.1039/d5ja00482a.

Abbreviations

CMOS	Complementary metal–oxide semiconductor
DL	Detection limit
ESL	Elemental scientific lasers
ICCD	Intensified charge-coupled device
ICP	Inductively coupled plasma
IFF	Interesting features finder
LA	Laser ablation
LIBS	Laser-induced breakdown spectroscopy
LOD	Limit of detection
LOQ	Limit of quantification
MSR	Molten salt reactor
OES	Optical emission spectroscopy
PC	Principal component
PCA	Principal component analysis
TQ	Triple quadrupole

Acknowledgements

The authors would like to acknowledge Jacquelyn Demink from Oak Ridge National Laboratory for assistance with graphics. This work was funded by the US Department of Energy's Office of Nuclear Energy, Advanced Reactor Development Program, Molten Salt Reactor Program. This research was performed using funding received from the US Department of Energy's Office of Nuclear Energy, Nuclear Energy University Program,

IRP-Project 23-30996, in conjunction with Virginia State University and Virginia Union University.

References

1 D. LeBlanc, Molten salt reactors: a new beginning for an old idea, *Nucl. Eng. Des.*, 2010, **240**(6), 1644–1656.
2 J. Serp, M. Allibert, O. Beneš, S. Delpech, O. Feynberg, V. Ghetta, D. Heuer, D. Holcomb, V. Ignatiev and J. L. Kloosterman, The molten salt reactor (MSR) in generation IV: overview and perspectives, *Prog. Nucl. Energy*, 2014, **77**, 308–319.
3 R. Roper, M. Harkema, P. Sabharwall, C. Riddle, B. Chisholm, B. Day and P. Marotta, Molten salt for advanced energy applications: a review, *Ann. Nucl. Energy*, 2022, **169**, 108924.
4 S. Guo, J. Zhang, W. Wu and W. Zhou, Corrosion in the molten fluoride and chloride salts and materials development for nuclear applications, *Prog. Mater. Sci.*, 2018, **97**, 448–487.
5 T. Hartmann and P. Paviet, Corrosion of containment alloys in molten salt reactors and the prospect of online monitoring, *J. Nucl. Fuel Cycle Waste Technol.*, 2022, **20**, 1738–1894.
6 S. S. Raiman and S. Lee, Aggregation and data analysis of corrosion studies in molten chloride and fluoride salts, *J. Nucl. Mater.*, 2018, **511**, 523–535.
7 H. B. Andrews, J. McFarlane, A. S. Chapel, N. D. B. Ezell, D. E. Holcomb, D. de Wet, M. S. Greenwood, K. G. Myhre, S. A. Bryan and A. Lines, Review of molten salt reactor off-gas management considerations, *Nucl. Eng. Des.*, 2021, **385**, 111529.
8 K. Goff, J. Wass and G. Teske, Electrochemical processing of used nuclear fuel, *Nucl. Eng. Technol.*, 2011, **43**, 335–342.
9 T. Inoue and L. Koch, Development of pyroprocessing and its future direction, *Nucl. Eng. Technol.*, 2008, **40**(3), 183–190.
10 K. Sridharan and T. Allen, Corrosion in molten salts, in *Molten Salts Chemistry*, Elsevier, 2013, pp. 241–267.
11 G. Chipman, B. Johnson, C. Vann, L. Whitesides and D. Rappleye, Experimental determination of the electrochemical properties of bismuth chloride in eutectic LiCl–KCl and LiCl–KCl–CaCl2 molten salts, *J. Radioanal. Nucl. Chem.*, 2024, **333**(3), 1119–1135.
12 N. C. Hoyt, C. A. Launiere and E. A. Stricker, In-process monitoring of molten salt composition by voltammetry and automated sampling-based techniques, *J. Nucl. Mater. Manag.*, 2021, **49**(1), 87–98.
13 S. D. Branch, H. M. Felmy, A. Schafer Medina, S. A. Bryan and A. M. Lines, Exploring the complex chemistry of uranium within molten chloride salts, *Ind. Eng. Chem. Res.*, 2023, **62**(37), 14901–14909.
14 H. B. Andrews, Z. B. Kitzhaber, D. Orea and J. McFarlane, Real-Time Elemental and Isotopic Measurements of Molten Salt Systems through Laser-Induced Breakdown Spectroscopy, *J. Am. Chem. Soc.*, 2024, **147**(1), 910–917.
15 Z. B. Kitzhaber, D. Orea, J. McFarlane, B. T. Manard and H. B. Andrews, Sparge Sampling of Molten Salts for Online Monitoring via Laser-Induced Breakdown Spectroscopy, *ACS Omega*, 2025, 37889–37897.
16 G. Cao, N. Larson, B. Storms, P. Kandlakunta, L. R. Cao and S. Li, Gamma-ray spectra analyses of molten salts in spent nuclear fuels pyroprocessing facilities for mass measurement, *J. Radioanal. Nucl. Chem.*, 2022, **331**(7), 3085–3091.
17 L. J. McIlwain, A. Leong, T. D. Bradshaw, A. A. Hromiak, S. J. Lopykinski, N. J. Condon and J. Zhang, Optimization of Oxygen and Hydrogen Analysis in Salts by Inert Gas Fusion, *Anal. Chim. Acta*, 2025, 344824.
18 A. Weisberg, R. E. Lakis, M. F. Simpson, L. Horowitz and J. Craparo, Measuring lanthanide concentrations in molten salt using laser-induced breakdown spectroscopy (LIBS), *Appl. Spectrosc.*, 2014, **68**(9), 937–948.
19 A. Limbeck, P. Galler, M. Bonta, G. Bauer, W. Nischkauer and F. Vanhaecke, Recent advances in quantitative LA-ICP-MS analysis: challenges and solutions in the life sciences and environmental chemistry, *Anal. Bioanal. Chem.*, 2015, **407**(22), 6593–6617.
20 T. Vaculovic, P. Sulovsky, J. Machat, V. Otruba, O. Matal, T. Simo, C. Latkoczy, D. Günther and V. Kanicky, The EPMA, LA-ICP-MS and ICP-OES study of corrosion of structural materials for a nuclear reactor cooling circuit by molten fluoride salt treatment, *J. Anal. At. Spectrom.*, 2009, **24**(5), 649–654.
21 E. H. Kwapis, J. Borrero, K. S. Latty, H. B. Andrews, S. S. Phongikaroon and K. C. Hartig, Laser ablation plasmas and spectroscopy for nuclear applications, *Appl. Spectrosc.*, 2024, **78**(1), 9–55.
22 B. T. Manard, C. D. Quarles Jr, V. C. Bradley, T. L. Spano, N. A. Zirakparvar, B. W. Ticknor, D. R. Dunlap, P. Cable-Dunlap, C. R. Hexel and H. B. Andrews, Uranium Single Particle Analysis for Simultaneous Fluorine and Uranium Isotopic Determinations via Laser-Induced Breakdown Spectroscopy/Laser Ablation–Multicollector–Inductively Coupled Plasma–Mass Spectrometry, *J. Am. Chem. Soc.*, 2024, **146**(21), 14856–14863.
23 A. Williams, *Zone Freezing Study for Pyrochemical Process Waste Minimization*, Idaho National Lab. (INL), Idaho Falls, ID, United States, 2012.
24 A. Williams, K. Bryce and S. Phongikaroon, Measurement of cerium and gadolinium in solid lithium chloride–potassium chloride salt using laser-induced breakdown spectroscopy (LIBS), *Appl. Spectrosc.*, 2017, **71**(10), 2302–2312.
25 H. Andrews and S. Phongikaroon, Electrochemical and laser-induced breakdown spectroscopy signal fusion for detection of UCl3-GdCl3-MgCl2 in LiCl-KCl molten salt, *Nucl. Technol.*, 2021, **207**(4), 617–626.
26 H. Andrews and S. Phongikaroon, Development of an experimental routine for electrochemical and laser-induced breakdown spectroscopy composition measurements of SmCl3 in LiCl-KCl eutectic salt systems, *Nucl. Technol.*, 2019, **205**(7), 891–904.
27 G. Hull, H. Lambert, K. Haroon, P. Coffey, T. Kerry, E. D. McNaghten, C. A. Sharrad and P. Martin, Quantitative prediction of rare earth concentrations in salt

matrices using laser-induced breakdown spectroscopy for application to molten salt reactors and pyroprocessing, *J. Anal. At. Spectrom.*, 2021, **36**(1), 92–102.

28 K. G. Myhre, H. B. Andrews, D. Sulejmanovic, C. I. Contescu, J. R. Keiser and N. C. Gallego, Approach to using 3D laser-induced breakdown spectroscopy (LIBS) data to explore the interaction of FLiNaK and FLiBe molten salts with nuclear-grade graphite, *J. Anal. At. Spectrom.*, 2022, **37**(8), 1629–1641.

29 P. T. Milota and S. Phongikaroon, Feasibility Study on Aluminum Under Laser Ablation for Corrosion Resistance in Molten Salt, *J. Nucl. Fuel Cycle Waste Technol.*, 2024, **22**(1), 67–80.

30 C. Paton, J. Hellstrom, B. Paul, J. Woodhead and J. Hergt, Iolite: Freeware for the visualisation and processing of mass spectrometric data, *J. Anal. At. Spectrom.*, 2011, **26**(12), 2508–2518.

31 H. B. Andrews, L. Hendriks, S. B. Irvine, D. R. Dunlap and B. T. Manard, TOFHunter—unlocking rapid untargeted screening of inductively coupled plasma–time-of-flight–mass spectrometry data, *J. Anal. At. Spectrom.*, 2025, **40**(3), 910–920.

32 P. Becker, J. Koch and D. Günther, Impact of ablation cell design in LA-ICP-MS quantification, *J. Anal. At. Spectrom.*, 2022, **37**(9), 1846–1854.

33 V. Palleschi, Avoiding misunderstanding self-absorption in laser-induced breakdown spectroscopy (LIBS) analysis, *Spectroscopy*, 2022, **37**(8), 60–62, DOI: 10.56530/spectroscopy.xq8876v9.

34 J.-M. Mermet, Limit of quantitation in atomic spectrometry: an unambiguous concept?, *Spectrochim. Acta, Part B*, 2008, **63**(2), 166–182.

35 J.-M. Mermet, Quality of calibration in inductively coupled plasma atomic emission spectrometry, *Spectrochim. Acta, Part B*, 1994, **49**(12–14), 1313–1324.

36 S. Phongikaroon and M. F. Simpson, Equilibrium model for ion exchange between multivalent cations and zeolite-A in a molten salt, *AIChE J.*, 2006, **52**(5), 1736–1743.